

# Flow Rate Computation of Highly Turbulent Pipe Flows using wide-band signals and matched filter-based approach in ultrasonic multi-element configuration

Teodor Petrut, Cornel Ioana, Andrei Anghel, Ion Candel, Gabriel Vasile  
Grenoble Institute of Technology, Saint Martin d'Hères, 38402, France  
[cornel.ioana, ion.candel, teodor-ion.petrut]@gipsa-lab.grenoble-inp.fr

## Abstract

Flow profile analysis and flow rate estimation with ultrasound Non-Destructive Testing (NDT) tools were performed in a pipe flow varying the Reynolds number from  $4.33 \cdot 10^5$  to  $1.67 \cdot 10^6$ . This study investigated the flow rate computation right downstream a  $90^\circ$  curvature pipe with a clamp-on multi-path ultrasonic flow meter (UFM) and a compensation scheme for the time-of-flight (TOF) errors due to the asymmetrical flow profile. The challenge is to model through the CFD analysis the separation region in the intrados of the pipe's elbow and its influence on the flow velocity profile, in order to calibrate the flow rate computations. The use of the matched filtering technique improves the performances in terms of measurement precision, which is validated by the numerical models. The experimental measurements on TOF differences in the pipe's elbow prove the interest of such approach for the improvement of the flow rate computations in the case of relative high turbulent flows.

**Keywords:** Non-destructive testing, ultrasonic flow meter, matched filter, time-of-flight, CFD analysis

## 1. Introduction

The commercial time-of-flight (TOF) ultrasonic flow meters (UFM) are gaining a lot of importance in the world of hydraulic metrology because they are portable, they do not physically affect the pipe structure and they are highly precise. It is worth to mention that the very common UFM achieve relative errors of about  $\pm 0.5-1\%$  only after following a set of pre-calibration tests (Hogendoorn et al., 2011). Still, their major usage constraint is that the device must be placed in a region of *fully-developed* pipe flow, i.e. at a distance of 20 pipe diameters downstream of any geometrical variation in the pipeline (Hanson et al., 1998). A solution to relax this constraint was to use the TOF multi-path UFM which models the asymmetrical flow in the under-developed flow region but even so, the constraint on measuring distance is still at least 10 diameters. More improvements were considered using artificial intelligence (Zhao et al., 2014) which brings the UFM up to 5 diameters from any irregularity.

More insights are given to the flow in unstable regions such as the region downstream a pipe's elbow. Several state-of-the-art approaches for treating highly unstable flow regions due to geometrical irregularities are proposed. Between them, it is worth to mention the UFM which uses multi-path beam propagation for velocity profile tomograms evaluation (Kurniadi et al., 2006). Instead of the inverse problem reconstruction, this research study uses the direct problem of CFD numerical modeling of flow profiles in order to cope with the pre-calibration and refinement of the flow rate computation precision. Therefore, the Computational Fluid Dynamics (CFD) commercial code ANSYS 14.5 Workbench was used for numerical modeling of the Dean vortices-type asymmetries which changes into a swirling flow across whole of the pipe.

The estimated location of the Dean vortices will be used to position a clamp-on US piezoelectrical transducers system, used to measure the difference in time-of-flight values across two

orthogonal ultrasound paths on the same cross-section. After that, another clamp-on transducers system used as an UFM will be calibrated assuming the previous errors, or differences, between the TOF values.

The paper is organized as follows. In Section 2, the theoretical issues are outlined and the validation of numerical experiments of modeling the flow downstream of the region of pipe's elbow is presented. In Section 3, the measurement principle used for the experimental validation is described. Simulation details and results in real context are presented in Section 4. Section 5 provides discussion and concluding remarks.

## 2. Theoretical issues

It is well known that the flow-induced vibration due to the piping geometry is caused mainly by the almost suddenly change in flow direction giving rise to great areas of recirculatory flow (zero-integral velocity) located in the intrados region of the pipe's elbow (A. Ono et al., 2011). The working frequencies of the ultrasound waves are normally not affected by these vibrations, however, it is the recirculatory regions, namely the Dean vortices which deform the flow profile in such a manner that flow rate measurement based on the use of single-path UFM gives systematical errors.

In order to clarify the Dean Vortex mechanism, it is important to study the mechanism of fluid flow pattern in the elbow. The flow separation always occurs right at the intrados of the elbow causing a large vortex downstream of it. In (A. Ono et al., 2011), two types of elbow of  $r/D = 1.0$  and  $1.5$  were used to investigate the influence of the elbow curvature on the separation point position. The results reveal that the separation point is located at  $x/D = 0.27$ , where  $x$  is the axial coordinate and in the case of the pipe's curvature radius of  $1 D$  and the averaged flow velocity of  $1\text{m/s}$ . However, for the same averaged velocity but with the bend's radius  $1.5D$ , as it is in this study case, the PIV images do not reveal any more such separation point. However It was proved by (Idelchik, 1986) that the bigger the flow velocity the farther downstream the pipe's elbow is the separation point. From the CFD analysis detailed in Section 3, the results represented in the Fig. 1 clearly show that the profile distortions are caused by the presence of a separation point located around  $1.5$  diameters downstream the elbow.

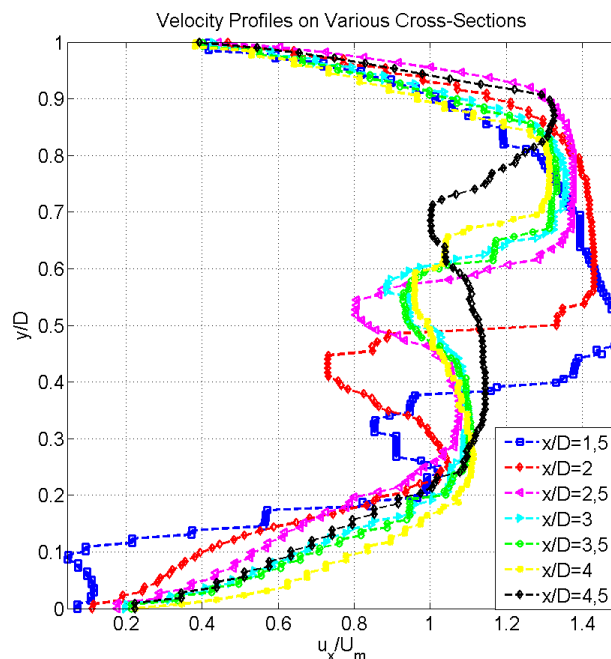


Fig. 1: Axial flow profiles from  $x/D = 1.5$  to  $x/D = 4.5 D$ , for a  $90^\circ$  bending pipe with  $r/D = 1.5 D$ . The studied flow rate in this case is  $250 \text{ m}^3/\text{h}$  which gives an averaged velocity on cross-section of  $1.97 \text{ m/s}$ .

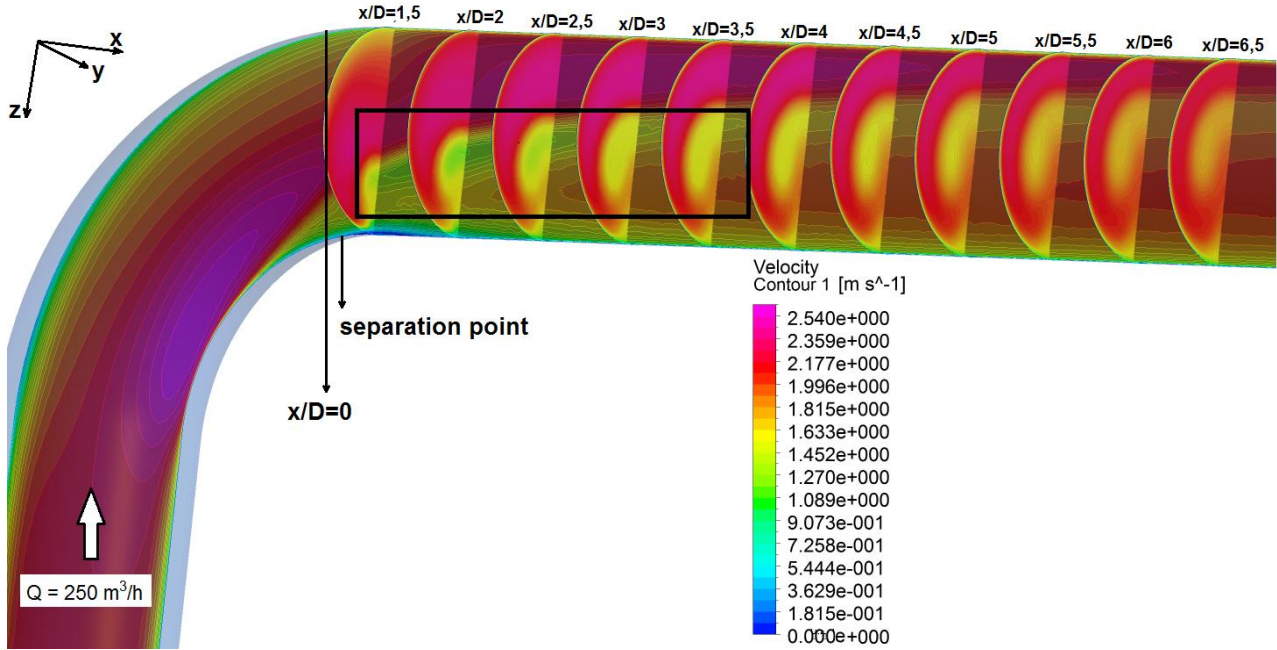


Fig. 2: The longitudinal flow profile predicted by CFD simulations; the separation point at is observed downstream the pipe's elbow; the numerical simulations considered an average velocity inlet equal to 1.97 m/s ( $Q = 250 \text{ m}^3/\text{h}$ ). The recirculatory region is marked by the black rectangle.

It is concluded that the separation point is very close to the elbow region and takes place at the same  $x/D$  as the one related by Idelchik's study. The recirculatory region is a quasi-stationary vortex located right in the pipe's intrados as it is observed in numerical simulation from the Fig. 2 and in Ono's study. It is observed that this vortex is a big flow structure relative to pipe's dimensions, responsible for the flow profile distortion so its precise location will be further used in this work to deal with the inherent errors of experimental measurements right after the pipe's elbow.

### 3. Numerical Simulation

The first issue was to decide the type of simulations: stationary or non-stationary. In (Y. Gao *et al.*, 2011) the numerical simulation were also conducted assuming a stationary flow, where the authors were looking for the best angle of measurement section. Giving the central frequency of an ultrasound pulse of 1 Mhz, it is clear that the pulse is way out of the Kolmogorov spectrum. Therefore, the fluctuating components of pressure and velocity are not at all interacting with the pulse's frequency so the non-stationary phenomena would exceed the scope of the article. Thus, the flow after the elbow will be considered stationary with average constant over time.

The geometry, shown in the Fig. 3b, is a 20 diameters  $90^\circ$  curved pips, with the diameter of 211.6 mm and the steel wall is of width 3.8 mm. During the study, 12 cross-sections were analyzed, all of them located downstream the pipe's elbow,  $z = \{1,5D; 2D; 2,5D; 3D; 3,5D; 4D; 4,5D; 5D; 5,5D; 6D; 6,5D; 8,5 D\}$ . The meshgrid consisted of 2 million tetrahedral cells and boundary layer was discretized according to the  $y^+$  factor.

The inlet boundary condition is set to be a turbulent profile distribution of velocities with the average velocity derived from three studied flow rates,  $Q = \{1000 \text{ m}^3/\text{h}; 500 \text{ m}^3/\text{h}; 250 \text{ m}^3/\text{h}\}$ . Thus, the average inlet velocities are  $V_m = \{7.9 \text{ m/s}; 3.8 \text{ m/s}; 1.7 \text{ m/s}\}$ . The outlet boundary condition is set as a pressure outlet of 4 bar.

This CFD solver is the ANSYS Workbench 14.5, a finite volume-based method for the integration of the incompressible Navier-Stokes equations through the SIMPLE (Semi-Implicit Method for Pressure Linked Equations) algorithm. The simulations used the Shear Stress Transport

turbulence model which combines the  $k-\omega$  turbulence model and  $k-\varepsilon$  turbulence model to simulate the inner region of the boundary layer and, respectively, the free shear flow region.

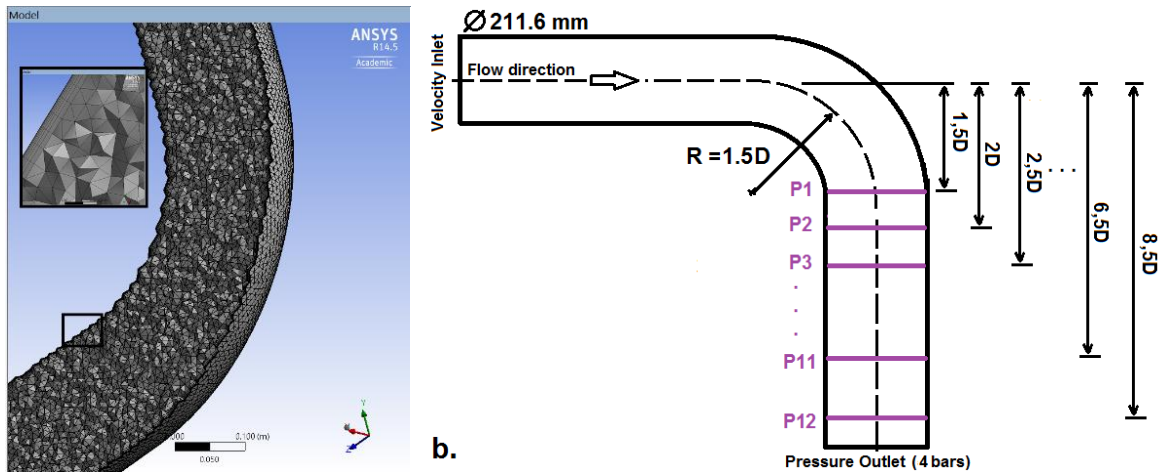
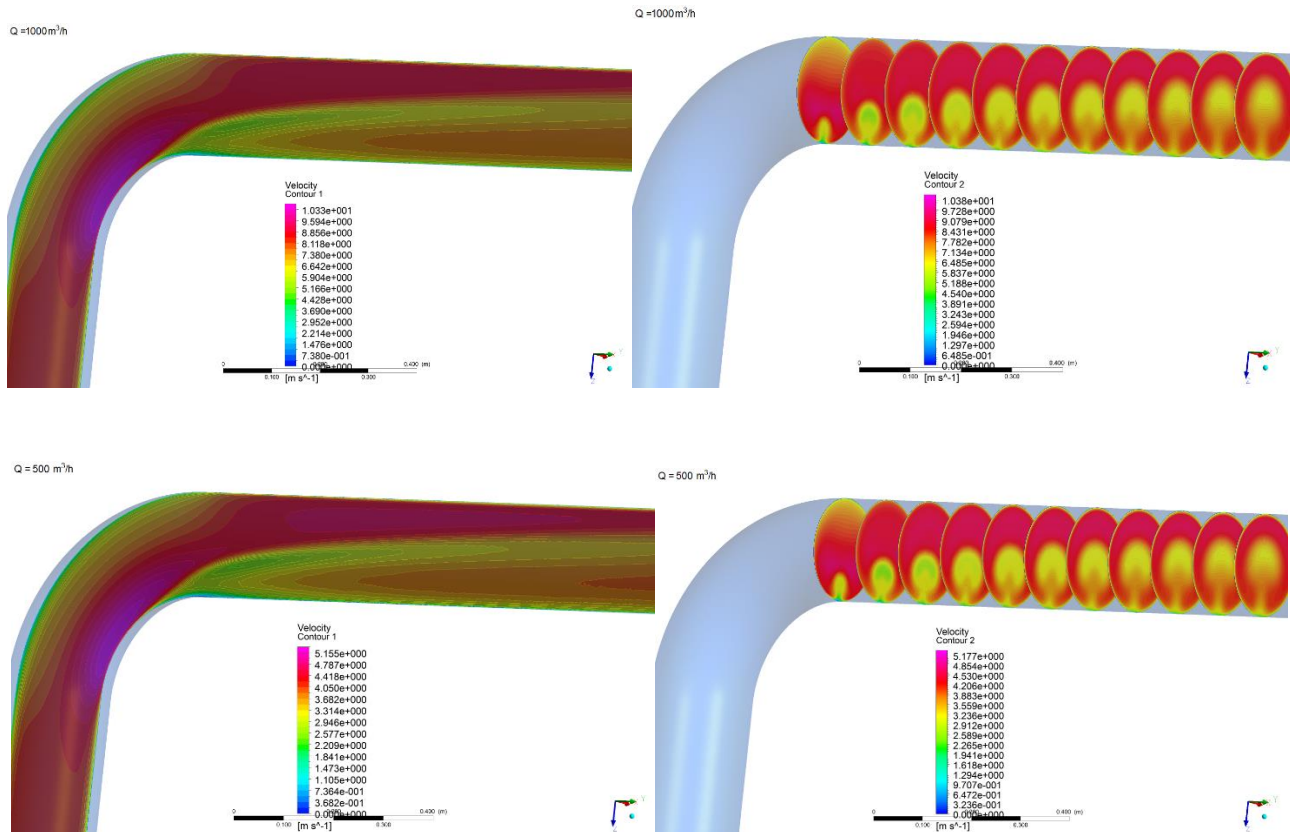


Fig. 3: The meshgrid (left) and the geometrical case with the boundary conditions used in numerical simulations

In the following figures, both the longitudinal and transversal flow velocity distributions are illustrated for three values of flow rates,  $Q = \{250 \text{ m}^3/\text{h}; 500 \text{ m}^3/\text{h}; 1000 \text{ m}^3/\text{h}\}$ . The longitudinal section is a cut section along the pipe's diameter and the 12 transversal monitoring planes, as pictured in Fig. 3b.



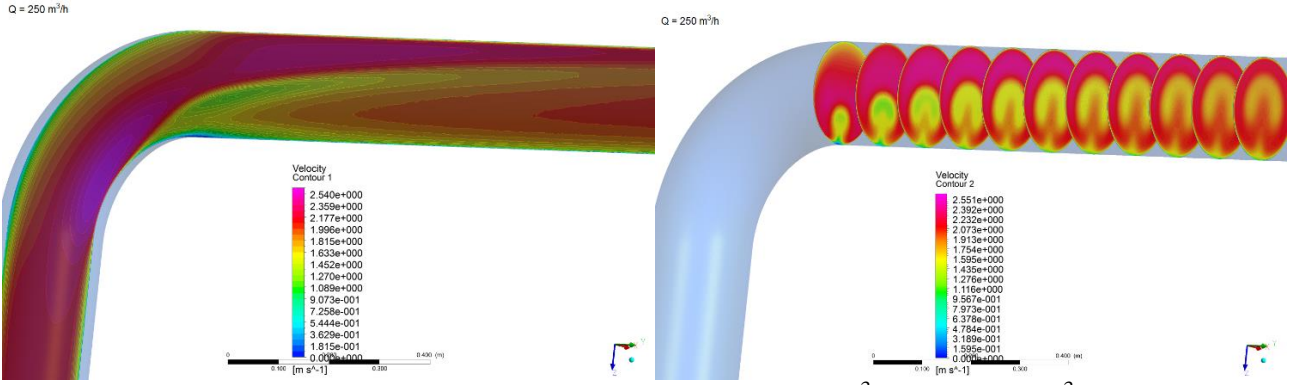


Fig. 4: The velocity contours for three modeled flow rates: 250 m<sup>3</sup>/h (top), 500 m<sup>3</sup>/h (center) and, respectively, 1000 m<sup>3</sup>/h (bottom) and monitoring cross-sections {P1...P11}

These numerical simulations confirm the theoretical prediction of the separation point location inside the elbow: the separation point is more upstream, for the lowest flow rate, than the higher flow rates. However, the location of the recirculatory stationary region is almost the same in the three cases, i.e. downstream the elbow in the intrados area. This location of the recirculatory phenomena will be further used in the study to assess the impact of fluid flow profile on the time propagation of ultrasounds, in the same cross-section, see section 5.

#### 4. Measurement Principle

The TOF UFM computes the flow rate by using a formula based on the difference between two pulses propagating in the two directions with respect of the flow along an ultrasonic path defined by the piezo-electric transducers. The streamwise pulse arrives earlier than the counter-streamwise pulse and, thus the time difference ( $\Delta T$ ) of their arrivals is directly proportional to the mean flow velocity.

In this work, the time difference is computed by using wide band signals and the Matched Filtering. Its governing equation is a convolution between the signal received and the reference, given by eq. (1), which is actually the emitted waveform. More details about the efficiency of the matched filter output in terms of Cramér-Rao bound are found in (Svilainis *et al.*, 2010). The value of  $\Delta T$  computed with the eq. (3) is further used in eq. (4), to compute the flow rate.

$$\langle s, r \rangle(t) = \int_0^{\infty} s^*(\tau) \cdot r(t + \tau) d\tau \quad (1)$$

$$T\hat{O}F_i = \arg \max_{t_i} \{ \langle s, r \rangle(t_i) \}, \quad i = 1, 2 \quad (2)$$

$$\Delta T = T\hat{O}F_2 - T\hat{O}F_1 \quad (3)$$

where  $s$  is the received signal,  $r$  is the reference signal,  $T\hat{O}F_2$  is the estimated time-of-flight of the US in the counter-streamwise direction and  $T\hat{O}F_1$  is the estimated time-of-flight in the streamwise direction. Using the  $\Delta T$ , the flow rate is expressed in eq. (4) as following:

$$Q = \underbrace{K_h}_{\text{Hydraulic coefficient}} \cdot \underbrace{\frac{c_{water}^2 \Delta T}{2 \cdot D \cdot ctg\left(\frac{\pi}{2} - \alpha_{US}\right)}}_{\text{Velocity}} \cdot \underbrace{\frac{\pi \cdot D^2}{4}}_{\text{Area of cross-section}} \quad (4)$$

where  $\alpha_{US}$  is the angle between the flow direction and ultrasound beam direction, computed using the Snell's formula, given by eq. (6);  $D$  – diameter of the pipe,  $D = 211,6$  mm in our experiment;  $c_{water}$  – the sound speed in water,  $K_h$  – hydraulic coefficient, is a calibration coefficient depending of the Reynolds number and

$$K_H = \frac{2 \cdot n + 1}{2 \cdot n}, \quad n = \frac{1}{0,25 - 0,023 \cdot \log Re} \quad (5)$$

$$\alpha_{US} = \arcsin\left[\frac{c_{water} \cdot \sin(\Theta_{E/R})}{c_{steel}}\right] \quad (6)$$

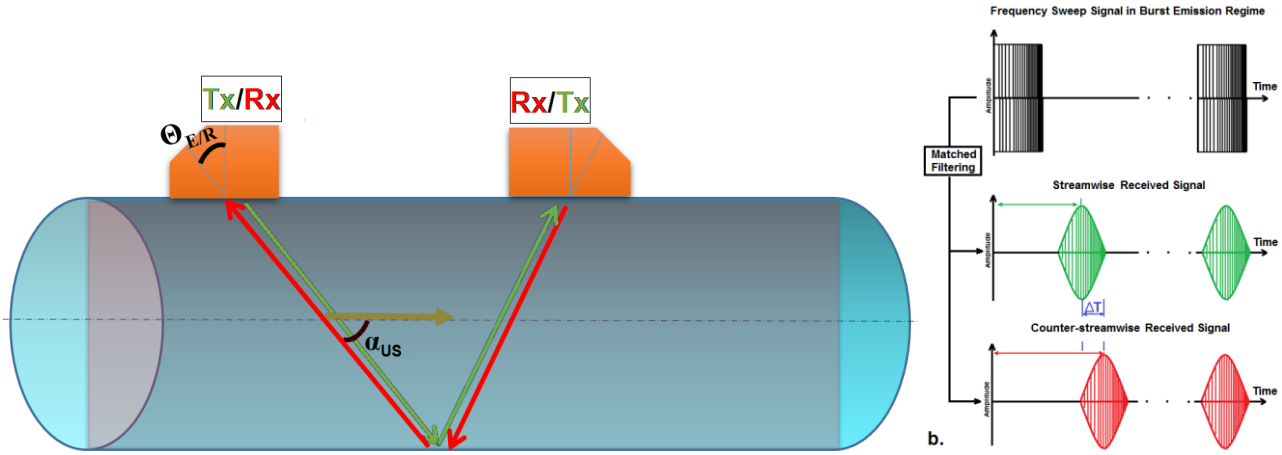


Fig. 5a The principle of flow rate measurement; b. The shape of the linear frequency modulated waveform used in emission, the shape of the received waveforms and the significance of difference of time arrival ( $\Delta T$ )

A classical method for flow rate computations is presented in Fig. 5a, from where it is noticed the two US angle beam transducers assembled on wedges, the configurable system of emission/acquisition and the PC for signal processing and flow rate computation. Besides, in the Fig. 6b it is shown the waveforms used in emission and the two receptions used for  $\Delta T$  computation by the matched filtering technique.

## 5. Experimental setup

The central idea of this paper is the flow rate computation improving using the wide band signals and flow profile analysis downstream the pipe's elbow. Thus, the experiments will consist in estimating the time-of-flight differences in the pipe's cross-section downstream the elbow, across two orthogonal ultrasound paths. The aim is to provide a compensating error for a UFM installed downstream the pipe's elbow.

The test rig, is composed by a pipeline with DN 211.6, 2-channel arbitrary function generator, a Matlab-controlled data acquisition system and 4 ultrasound piezo-electrical transducers. The two ultrasound paths are orthogonal between each other and they are defined by 4 normal incidence transducers placed around the pipe's circumference. The location of these transducers is

chosen according to the position of the recirculatory region, or Dean vortices, located in the pipe's elbow intrados, as shown in Fig. 7b.

Another upgrading of the experimental test rig is the installation of another four angle beam in-line transducers two paths which propagate ultrasound across "V" path configuration, also pictured

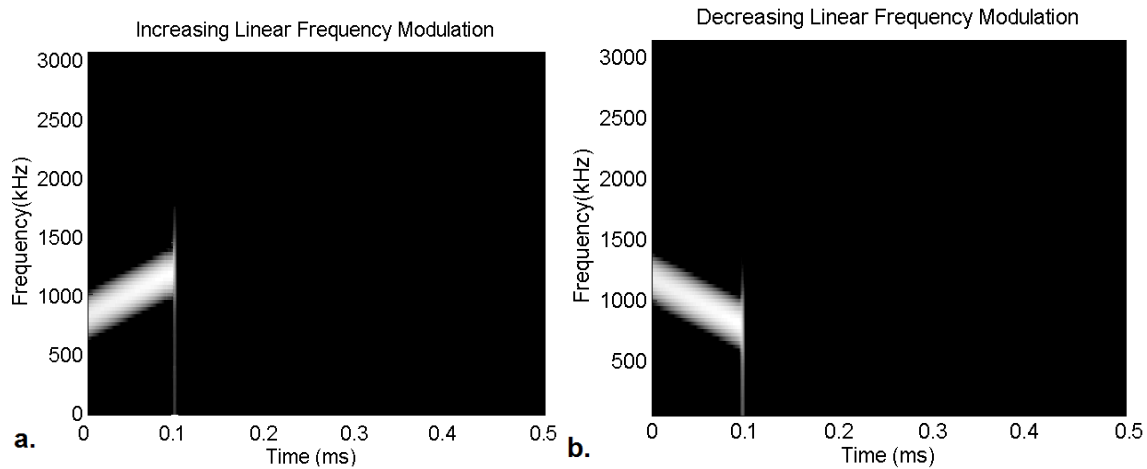


Fig. 6a-b: Spectrograms of the waveforms used for the two simultaneous emissions along two crossing ultrasound paths

in the Fig. 7a. The two "V" paths are used to simultaneously compute direct and invers transit times without the need of physically switching between emission and reception. To do so and, in order to avoid the interferences between the two ultrasonic paths, two types of frequency modulations are used increasing linear frequency modulations and decreasing linear frequency modulation, respectively. The Fig. 6a-b illustrates the spectrogram of the both linear frequency modulations.

There are two methodical stages to follow during such experiment: the first stage computes the error of the estimated time-of-flight of the two orthogonal ultrasound paths for the pre-calibration part of the second stage. As long as one considers the case of a developed turbulent flow profile, the two time-of-flight, computed within the same cross-section, would be the same because of the symmetry of the velocity profile. On the other hand, the presence of an asymmetrical flow profile intuitively imposes a difference between the two time-of-flight values and this difference will be considered as the compensating error for flow rate computations by the UFM.

The ultrasound transducers used in the experiments, illustrated in the Fig. 7a, have the central frequency of 1 MHz and the surface of the active element is 769 mm<sup>2</sup>. The time-of-flight values computed in the no-flow regime are the same along the two orthogonal paths and their relative error is 0.75%, compared to the theoretical time-of-flight, which is 144,3 μs for a 219,2 mm external diameter pipe.

The Ultrasonic Flow Meter, shown in Fig. 8a, is designed to simultaneously measure the two bi-directional time-of-flight values. It is composed by another 4 angle-beam ultrasound transducers, illustrated in the Fig. 8b, whose central frequency is also 1 MHz and active element has 910 mm<sup>2</sup>.

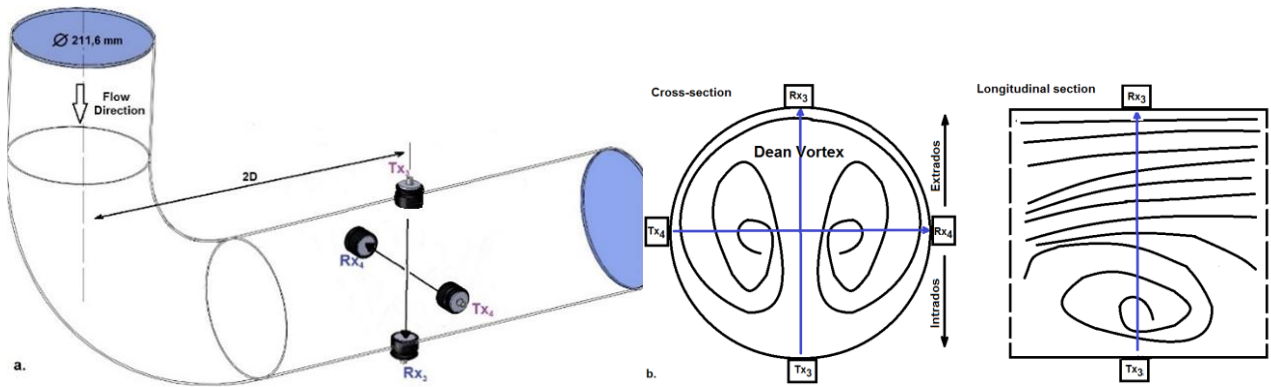


Fig. 7a: The real-scale experimental setup with the positions of normal incidence piezo-electrical transducers (the arrows represent the front wave propagation directions); b. The positions of the ultrasound transducers TX<sub>3</sub>, TX<sub>4</sub>, RX<sub>3</sub> and RX<sub>4</sub>, where Tx - emitter end Rx - reception, with respect to the Dean vortices' positions.

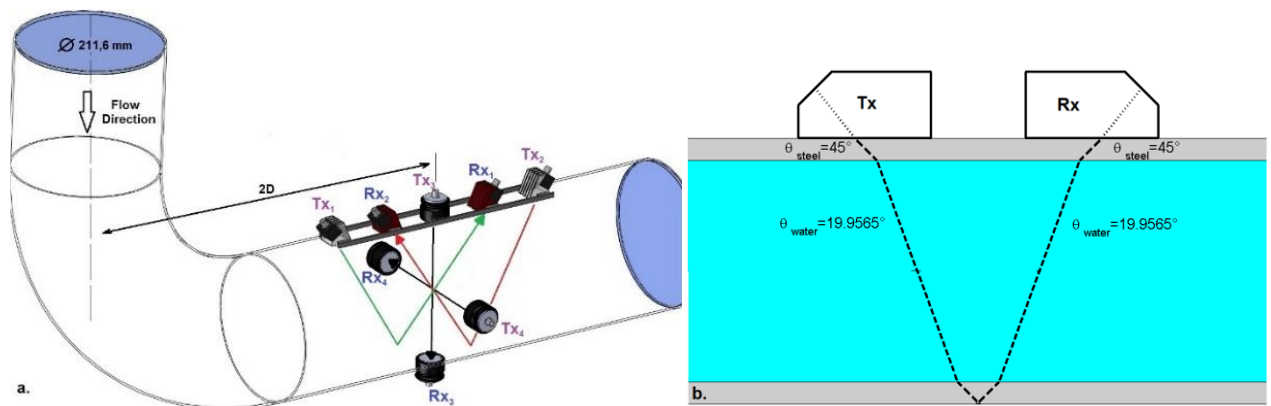
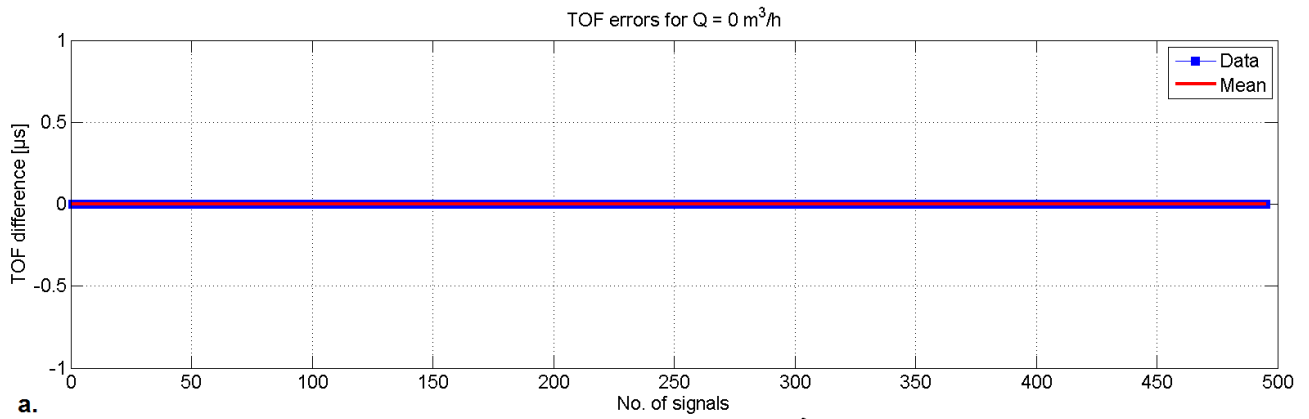


Figure 8a: The real-scale experimental setup with the position of the ultrasonic flow meter made of in-line angle beam ultrasound transducers ((TX<sub>1</sub>, TX<sub>2</sub>, RX<sub>1</sub>, and RX<sub>2</sub>); b. The refraction angles computed using the Snell's law related in eq. (6)

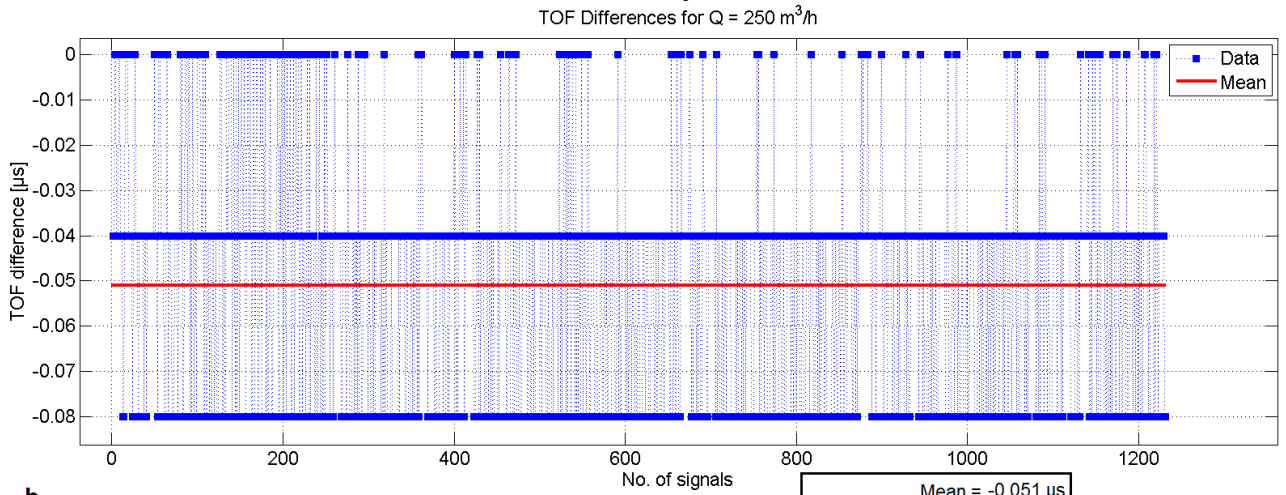
## 6. Discussion of results

The signal processing technique applies the matched filtering. Two kind of waveforms are used: a 800-1200 kHz linear increasing sweep frequency signal, injected in TX<sub>1</sub> and TX<sub>3</sub>, and a 800-1200 kHz linear decreasing sweep frequency signal, injected in TX<sub>2</sub> and TX<sub>4</sub>, both signals' spectrograms being rendered in Fig. 6a. The sampling frequency is 25 MHz (0.04  $\mu$ s of temporal resolution), which is considered to be enough for sensing flow rates down to 30 m<sup>3</sup>/h. The angle wedges are designed to give a 45° refracted beam in the pipe wall steel.

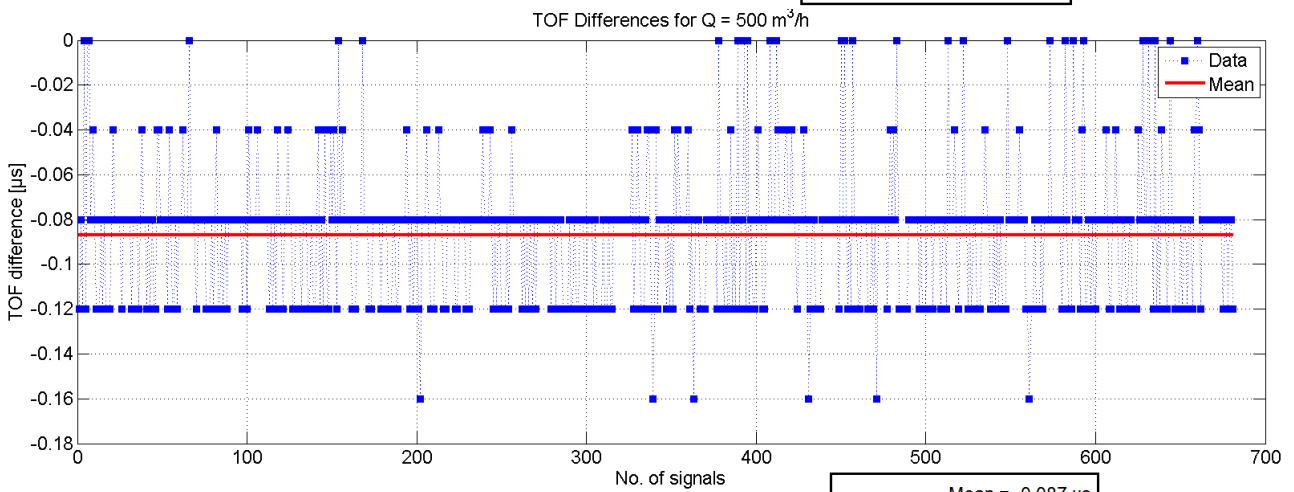
The time-of-flight values measured by the transducers RX<sub>3</sub> and RX<sub>4</sub> are used to compute the differences between the two TOFs. Before testing for different flow rates, the static condition is analyzed and it was confirmed that all the measurement gave 0 difference between the time-of-flights, as in the Fig. 9a. The graphs shown in the Fig. 9b-d, prove that the averaged of TOF differences and the standard deviation of this value rise when the flow rate is increased. This is explained because the intensity of the rotational vortex becomes higher with the increasing of the flow rate.



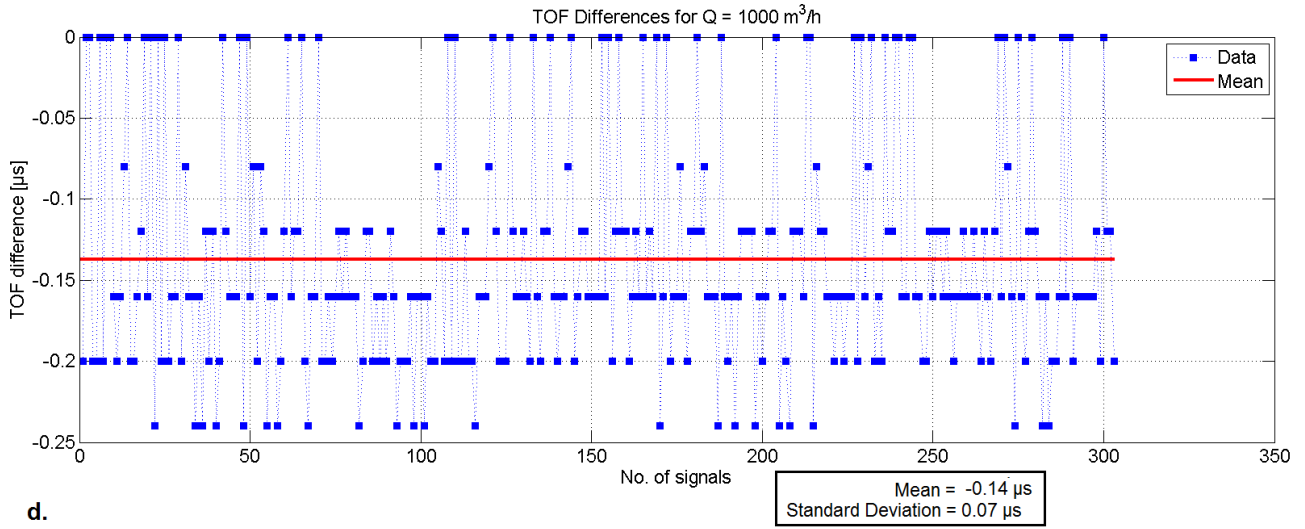
a.



b.



c.



d.

Fig. 9a-d: The differences in time-of-flight values measured by Rx<sub>3</sub> and Rx<sub>4</sub>. The mean and the standard deviation on the measured data reveal the same rising trend with the increase of the flow rate; a. the no flow case; b. the flow rate of 250 m<sup>3</sup>/h; c. the flow rate of 500 m<sup>3</sup>/h; d. the flow rate of 1000 m<sup>3</sup>/h;

It is clear from the Fig. 9b-d that there is a correlation between the increasing of the flow rate and the rise in error of the time-of-flight computation within a cross-section. The no flow case gives the zero mean in time-of-flight differences as it is normal. Beginning with lowest tested flow rate of 250 m<sup>3</sup>/h, the averaged absolute value of TOF difference was of -0.051 µs, for the flow rate of 500 m<sup>3</sup>/h the difference was of -0.087 µs and, finally, the highest tested flow rate of 1000 m<sup>3</sup>/h revealed a difference of -0.14 µs. It should also be noticed that the same correlative trend with respect to flow rate evolution is observed for the standard deviations of measurements. Another interesting fact is that the same sign TOF differences are due to the fact that the ultrasound path passes through the same half region of the rotational vortex, no matter the flow rate. The negative values will give negative flow rates which are non-physical because the flow meter equation, defined in eq. (4), always takes into consideration that the counter-streamwise TOF takes longer than the streamwise TOF.

The TOF differences across the orthogonal sound paths are further used in the flow meter equation to estimate the flow rates associated to those differences. These values of flow rate will be considered as the errors and used for the UFM calibration, following the eq. (10). The UFM, as already illustrated in the Fig. 8a-b, was calibrated *a priori* in normal conditions of use (50 diameters from any geometrical irregularity) so it is assumed that the errors due to other causes than the pipe's elbow flow are very small (~1%). The 45° angle beam transducers gives  $\alpha_{\text{water}} = 20^\circ$  so the computations for each respectively TOF difference is given using the eq. (4):

$$Q_{\text{error}_{250}} = -\frac{2 \cdot \frac{1}{0,25 - 0,023 \cdot \log 416900} + 1}{2 \cdot \frac{1}{0,25 - 0,023 \cdot \log 416900}} \cdot \frac{1500^2 \cdot 51 \cdot 10^{-9} \cdot 3600}{2 \cdot 0.2116 \cdot \text{ctg}\left(\frac{\pi}{2} - 20^\circ\right)} \cdot \frac{\pi \cdot 0.2116^2}{4} = -85.9 \text{ m}^3 / \text{h} \quad (7)$$

$$Q_{\text{error}_{500}} = -144.6 \text{ m}^3 / \text{h} \quad (8)$$

$$Q_{\text{error}_{1000}} = -229.7 \text{ m}^3 / \text{h} \quad (9)$$

$$Q_{\text{calibration}} = Q_{\text{UFM}} + Q_{\text{error}} [\text{m}^3 / \text{h}] \quad (10)$$

where  $Q_{UFM}$  is the raw flow rate measurement given by the UFM,  $Q_{error}$  is the flow rate computed with eq. (4) but using the differences between TOF on the pipe's cross-section and  $Q_{calibration}$  is the adjusted flow rate.

The  $Q_{error}$  values from the eq. (7)-(9) represent the flow rate specific to their respectively differences of TOF values computed with the matched filtering technique and in the same cross-section. Thus, a difference in TOF due to asymmetrical profile gives a non-physical flow rate of -85.9 m<sup>3</sup>/h. For a reference flow rate of 250 m<sup>3</sup>/h, the designed UFM measured 164 m<sup>3</sup>/h. In the next table, the errors of flow rate measurement for all of the three flow rates are presented, in conditions without and with calibration with the pre-computed TOF differences across orthogonal sound paths. It was assumed no *repeatability* error study during experiments.

Nominal flow-rate	Computed flow-rate	Relative error	Adjusted flow rate	Relative error after adjusting
250 m <sup>3</sup> /h	164 m <sup>3</sup> /h	34.4%	258 m <sup>3</sup> /h	3.2 %
500 m <sup>3</sup> /h	355 m <sup>3</sup> /h	29 %	516 m <sup>3</sup> /h	3.2%
1000 m <sup>3</sup> /h	770 m <sup>3</sup> /h	23%	977 m <sup>3</sup> /h	2.8%

Table I: The relative errors measured after the pipe's elbow including/not including the pre-calibration using the time-of-flight differences along the same cross-section's sound paths

The results from the table I reveal the improvement of the flow rate computations using the presented UFM. The errors are decreased with an order of magnitude and the bigger the flow rate the more precise are the results.

## 7. Conclusions

The presented research study brought into attention a method for pre-calibrating an experimental ultrasonic device for flow rate computations in the very proximity of a pipe elbow. The classical ultrasonic flow meters are limited with respect to the precision of flow rate computation because the assumption of the symmetrical flow profile cease to exist right after the bending pipe. The solution brought by this study was to use the a priori computation of time-of-flight error in order to compensate the flow meter estimation of flow rate. It was proved that the numerical analysis by CFD could bring relevant informations about the flow structure after irregular piping geometries which can improve the precision of flow rate measurements by UFM systems. Following the adjustment approach used in this work, the relative errors were brought to reasonable absolute values, between 2% and 3%. Given the instrumentation adopted during the experiments, it is considered that further improvement will be achieved if more ultrasound paths on a cross-section will be used for velocity profile analysis.

Acknowledgement: This work has been funded by the FUI-Tenerrdis project "Smart Hydro Monitoring". The authors are thankful to the EDF R&D Chatou (France) for the access and full support in using their experimental facility. The authors are also thankful to the researchers of Power Faculty of University "Politehnica" of Bucharest for their help in simulations using ANSYS software.

## References

1. B. R. Hanson and L. J. Schwankl, Error Analysis of Flow Meter Measurements, *Journal of Irrigation and Drainage Engineering*, Vol. 124, No. 5, Sept.-Oct. 1998, pp. 248-256;
2. Holm M., Stand. J., Delsing J., Simulation of flow meter calibration factors for various installation effects, *Measurement 15*, pp. 235-244, 1995;

3. H. Zhao, L. Peng, T. Takahashi, T. Hayashi, K. Shimizu, T. Yamamoto, ANN Based Data Integration for Multi-Path, Ultrasonic Flowmeter, *IEEE Sensors Journal*, Vol. 14, No. 2, February 2014, pp. 362-370;
4. D. Kurniadi, A. Trisnobubi, A multi-path ultrasonic time flow meter using a tomography method for gas flow velocity profile measurement, *Particle and Particle Systems Characterization*, vol. 23, no. 3-4, 2006, pp. 330–338.
5. A. Ono, N. Kimura, H. Kamide, A. Tobita, Influence of elbow curvature on flow structure at elbow outlet under high Reynolds number condition, *Nuclear Engineering and Design*, Vol. 241, 2011, 4409–4419
6. Y. Gao, Y. Zheng, Flow Analysis of Circular Bent Pipe Based On Numerical Simulation, *Electrical and Control Engineering (ICECE)*, 16-18 Sept. 2011, pp. 669 - 672;
7. L.Svilainis, P. Kabišius, S. Kitov, Ultrasonic transit time flow meter for diesel: initial analysis, *Ultragarsas (Ultrasound)*, Vol. 65, No. 4, 2010, pp. 16-21;
8. I. E. Idelchik, Handbook of Hydraulic Resistance, Second Edition, *Hemisphere Publishing Co.*, 1986;
9. J. Hogendoorn, H. Hofstede, P. van Brakel and A. Boer, How Accurate are Ultrasonic Flowmeters in Practical Conditions; Beyond the Calibration, *NSWMMF11*, 2011;